Fire Resistance of Tunnel Liners with Steel and Polypropylene Fibers

FINAL PROJECT REPORT

By

Saidong Ma,
Spencer Quiel,

Clay Naito
Email: cjn3@lehigh.edu
Lehigh University

Lehigh University

Sponsorship
U.S. Department of Transportation
Lehigh University Cost Share Support

For

University Transportation Center for
Underground Transportation Infrastructure
(UTC-UTI)

October 2023

Disclaimer

The contents of this report reflect the views of the authors, who are responsible for the facts and the accuracy of the information presented herein. This document is disseminated in the interest of information exchange. The report is funded, partially or entirely, by a grant from the U.S. Department of Transportation's University Transportation Centers Program. However, the U.S. Government assumes no liability for the contents or use thereof.

1. Report No. LUY6T1	2. Government Accession No.	3. Recipient's Catalog No.	
4. Title and Subtitle Fire Resistance of Tunnel Liners with Steel and Polypropylene Fibers		5. Report Date December 2023 6. Performing Organization Code	
7. Author(s) Saidong Ma: https://orcid.org/0000-0001-6907-2801, Spencer Quiel: https://orcid.org/0000-0002-1316-7059, Clay Naito: https://orcid.org/0000-0003-3835-8131,		8. Performing Organization Report No. LU - Year 6 - Task 1	
9. Performing Organization Name and Address University Transportation Center for Underground Transportation Infrastructure (UTC-UTI) Tier 1 University Transportation Center Colorado School of Mines Coolbaugh 308, 1012 14th St., Golden, CO 80401		10. Work Unit No. (TRAIS) 11. Contract or Grant No. US DOT Grant # 69A3551747118	
12. Sponsoring Agency Name and Address United States of America Department of Transportation Research and Innovative Technology Administration		13. Type of Report and Period Covered Final Report (Oct. 2021 to Dec. 2023) 14. Sponsoring Agency Code UTC-UTI Colorado School of Mines	
15. Supplementary Notes Report also available at: https://zenodo.org/communities/utc-uti			
16. Abstract This study aimed to assess the influence of polypropylene fibers on the fire resistance of steel fiber-reinforced concrete tunnel linings. Four distinct concrete mixtures were selected for comparison. The first mix contained only steel fibers and served as the control group. The subsequent three mixes incorporated varying amounts and lengths of polypropylene fibers based on the control mixture. For each mix, two concrete specimens of dimensions 150×457×610 mm were cast. All specimens were subjected to vertical loading at 20% of the design level of uniaxial compressive stress. The specimens were exposed to high temperatures using a gas radiant panel for single-sided heating. The results revealed that the concrete containing only steel fibers experienced complete spalling within 2.5 minutes. Conversely, the specimens with 1kg/m³ of 6mm polypropylene fibers displayed minimal spalling. The other two mixes with polypropylene fibers exhibited no thermally-induced spalling. These findings suggest that the inclusion of polypropylene fibers significantly enhances the fire resistance of concrete tunnel linings, offering a new perspective for tunnel safety. Additionally, temperature-time histories were recorded for a 25 mm thickness on the exterior of the heated concrete. These findings offer valuable insights for the design of fire-resistant concrete tunnel linings.			
17. Key Words Steel fiber-reinforced concrete, Polypropylene fibers, Fire resistance, Tunnel lining		18. Distribution Statement No restrictions.	
19. Security Classification (of this report) Unclassified	20. Security Classification (of this page) Unclassified	21. No of Pages 99	22. Price NA

Table of Contents

List of Figures 5

List of Tables 6

List of Abbreviations 7

Executive Summary 8

Chapter 1 Introduction and Background 10

Chapter 2 EXPERIMENTAL PROGRAM 14

2.1. Panel Specimen 14

2.2. Test Setup 18

2.3. Thermal Exposure 21

2.4. Applied Axial Loading 25

Chapter 3 Results and Discussion 27

3.1. Panel Test 27

3.2. Temperature Time History 30

Chapter 4 Conclusion 34

REFERENCEs 35

APPENDIX A – Technology Transfer Activities 40

LIST OF FIGURES

Figure 1: Concrete specimen details: (a) front view and (b) side view; (c) specimen formwork and (d) thermocouple placement for panels 15
Figure 2: Fibers (a) steel fibers, (b) Bekaert PP fibers, and (c) Nycon PP fibers 16
Figure 3: Concrete heat and loading frame 18
Figure 4: Self-reacting axial and heating load frame 20
Figure 5: Testing apparatus heat flux calibration setup 22
Figure 6: Reflector box 23
Figure 7: Radiant heat flux calibration for different radiant panel face configurations and ASTM E1529 hydrocarbon fire values 23
Figure 8: Heat flux percentage contour [%] 25
Figure 9: Axial load history during each test: (a) first 5 min, and (b) up to 50 min. 26
Figure 10: Water seepage on concrete panel during heat exposure 27
Figure 11: Panels without polypropylene fibers (SP0) 28
Figure 12: Panels with 2kg/m^2, 6mm long polypropylene fibers (SP2L6) 29
Figure 13: Panels with 1kg/m^2, 6mm long polypropylene fibers (SP1L6) 30
Figure 14: Panels with 1kg/m^2, 19mm long polypropylene fibers (SP1L19) 31
Figure 15: Temperature history recorded through the thicknesses of each specimen: (a) surface, (b) 6.4mm and (c) 12.7mm 32
Figure 16: Surface temperature during the first 3 minutes of heating 33

LIST OF TABLES

Table 1: Fiber parameters 15
Table 2: Summary of concrete mix design and thermo-mechanical properties..... 16
Table 3: Summary of pre-test panel specimen conditions 17
Table 4: Average heat flux..... 24
Table 5: Summary of heated panel test results. 28

LIST OF ABBREVIATIONS

SFRC: Steel Fiber Reinforced Concrete

PP: Polypropylene Fiber

MC: Moisture Content

RH: Relative Humidity

GGBFS: Granulated Blast Furnace Slag

SSD: Saturated Surface Dry

SG: Specific Gravity

EXECUTIVE SUMMARY

Tunnels, as semi-enclosed structures, are highly susceptible to elevated risks during fire incidents. Of particular concern are the deteriorating mechanical performance of tunnel concrete linings and potential thermal spalling at high temperatures. This necessitates costly post-fire replacements of the concrete lining and closure of lanes and bores, resulting in significant economic ramifications.

Traditional reinforcement methods have increasingly incorporated steel fibers in concrete linings. In contrast to conventional rebar, steel fibers, dispersed uniformly throughout the concrete matrix, offer multi-directional crack resistance and enhanced compactness by effectively controlling the propagation of micro-cracks. Current research indicates that while steel fibers enhance some fire-resistance aspects, they are insufficient in preventing thermal spalling of concrete.

Polypropylene (PP) fibers, known for their low melting point, hold substantial potential in curbing thermal spalling. This study revolves around four concrete mix designs, with the established steel fiber concrete mix for ongoing tunnel construction serving as the baseline and control group. The other mixes incorporated PP fibers in different quantities and lengths: 2kg/m^3 (6mm in length), 1kg/m^3 (6mm in length), and 1kg/m^3 (19mm in length). For each mix design, two concrete panels measuring 150 mm in thickness, 457 mm in width, and 610 mm in height were cast. These specimens were subjected to an axial compressive load at 20% of design strength of concrete and exposed to thermal fluxes akin to ASTM E1529 standards using a natural gas burner. Moisture content, internal relative humidity, and ambient temperature were recorded prior to testing. Specimens without PP fibers invariably experienced thermal spalling, while those integrated with PP fibers showcased minimal to no spalling. This study also shows temperature-time history and the measured damage depths.

In conclusion, the inclusion of PP fibers in tunnel concrete linings presents a promising avenue towards enhancing fire resilience, thereby potentially saving significant post-fire repair costs and minimizing infrastructure downtime.

Findings

The primary focus of this experiment was to assess the influence of PP fibers of varying lengths and dosages on the spall resistance capability of steel fiber-reinforced concrete used in tunnel linings.

Under ASTM E1529 hydrocarbon fuel fire exposure of 1 hour, the steel fiber-reinforced concrete specimens without added polypropylene fibers demonstrated multiple instances of thermal spalling within the initial 2.5 minutes of heating. For the concrete specimens with PP fibers:

- One specimen integrated with 1kg/m^3 of 6mm length PP fibers manifested only minimal spalling.
- No spalling was observed in the other two mixes with different PP fiber lengths and dosages.
- A higher dosage and longer length of PP fibers imparted enhanced resistance to spalling during fires.

Concrete panels that did not initially spall during the fire exposure started to show progressive surface degradation after being left exposed to ambient conditions for an extended period. This highlights the latent thermal damage and underscores the necessity to replace the thermally compromised outer layer of the concrete post-fire.

CHAPTER 1 INTRODUCTION AND BACKGROUND

Concrete is extensively used in structures, such as buildings, bridges, and tunnels. In tunnel construction, due to their semi-enclosed nature, the internal temperature of a tunnel can rapidly rise in the event of a fire, causing significant thermal impact on the tunnel lining concrete [1,2] . This rapid temperature increase irreversibly affects the strength, stiffness, and durability of concrete [3–5], and can also lead to concrete spalling [4,6]. Spalling not only affects the structural integrity, reducing load-bearing capacity but also may expose reinforcement within the concrete to high temperatures, accelerating the thermal-mechanical strength loss of the system. Thermal induced spalling of concrete poses a serious threat to structural safety.

Thermal induced concrete spalling refers to the process where fragments of surface concrete break off from the main mass when subjected to a severe thermal exposure [7–9]. The causes of concrete spalling are complex, involving intrinsic properties of the concrete, such as pore structure and water content, as well as external factors such as fire size [10] and ventilation conditions [11]. To prevent spalling, various methods [6,12–14] can be adopted including reducing the water-cement ratio, using high-performance concrete to improve fire resistance and crack resistance, applying fireproof coatings on concrete surfaces, and incorporating polypropylene fibers.

Steel fiber reinforced concrete (SFRC) is a composite material that integrates a cementitious matrix with discontinuous, randomly distributed steel fibers. SFRC is increasingly employed in the production of both in-situ and precast concrete structures. In elements subjected to overall compression, it sometimes completely replaces traditional reinforcement, such as ground support slabs, tunnel linings, foundations, and thin-shell structures [15–17]. Particularly notable for its overall durability and compressive strength, the use of steel fibers as a partial or complete replacement for traditional reinforcement has emerged as a popular solution in the construction of tunnel segmental linings. This innovative approach enhances structural performance while optimizing material usage [18–20]. However, the effectiveness of steel fibers in enhancing the explosive spalling resistance of concrete under fire conditions remains a subject of debate [21–24]. While some studies indicate potential improvements, comprehensive evaluation and consensus in the field are still evolving.

The mechanisms of concrete spalling at high temperatures typically fall into three categories: thermo-hygral spalling, thermo-mechanical spalling, and thermo-chemical spalling [25].

Thermo-hygral spalling occurs in a process where, upon exposure to fire, a temperature gradient is formed in the area close to the heated surface of the concrete. As the temperature rises, gel water and chemically bound water are released into the concrete's micropores and added to the free water [26]. Due to the increase in temperature and the presence of water (both liquid and vapor), pore pressure gradually increases [27,28]. Pressure gradients are formed due to the temperature gradient and pore saturation. This gradient drives the moisture in two opposite directions: towards the heated surface and towards the deeper, cooler regions. Consequently, three distinct zones are formed: the dry zone, the wet zone, and the saturated zone (the so-called moisture clog) [25]. When peak pressure exceeds the tensile strength of concrete at high temperatures, explosive spalling occurs. This mechanism typically operates in the temperature range of 220°C to 320°C [25], and is often characterized by explosive spalling.

Thermo-mechanical spalling is caused by thermal stresses due to temperature gradients between the heated surface and the interior of the concrete [29–33]. The surface layer of concrete is under a state of biaxial compression parallel to the heating surface and tension perpendicular to it. Additionally, the incompatibility of strains between the aggregate and cement matrix, along with shrinkage of the cementitious matrix due to water evaporation, causes tensile stresses that exceed the concrete's tensile strength, leading to thermomechanical spalling. This type of spalling typically occurs in the temperature range of 430°C to 660°C [25]. Concrete spalling is often the result of a combination of factors including pore pressure, thermal gradients, and the reduced mechanical properties of concrete at high temperatures [6].

Thermo-chemical spalling can occur at considerably high temperatures, or during the cooling phase after a fire. At elevated temperatures, the decomposition of compounds such as calcium hydroxide, calcium silicate hydrates, and calcareous aggregates leads to a reduction in the bonding strength between the aggregate and the cement [5,25,34]. Above 800°C, the quantity of calcium silicate hydrate (C-S-H) gel significantly diminishes [35]. During the cooling phase, the decomposition of calcium carbonate in calcareous aggregates produces calcium oxide. The calcium oxide in the surface layers then rehydrates with moisture from the air, causing expansion and severe cracking, which subsequently leads to concrete spalling. Post-fire spalling during the

cooling phase is a gradual process. If calcium oxide remains in the deeper layers of the concrete, it continues to react with moisture from the air, and this process can continue for several weeks. The prolonged nature of this reaction contributes to the progressive degradation and spalling of the concrete structure.

To mitigate spalling, many efforts have been done. One effective method to prevent concrete spalling is the addition of polypropylene (PP) fibers [36–41]. Polypropylene fibers, produced from polypropylene polymers (a type of thermoplastic resin), are known for their low density and good tensile strength, finding widespread application in various fields [42]. Their use in concrete to prevent spalling is primarily due to their melting temperature. Typically, PP fibers begin to melt around 150°C and completely liquify between 160°C and 170°C [42]. Additionally, PP fibers also undergo thermal expansion resulting in incompatibility with the cement matrix and creation of microcracks within the concrete [42]. When heated, the melted PP fibers flow into the pores and cracks of the cementitious material, and the spaces previously occupied by the fibers are replaced by empty channels [43,44], facilitating the evacuation of water vapor. This results in an observed increase in permeability [45] and a reduction in peak pore pressures internally [46], thus lowering the risk of spalling. Furthermore, PP fibers can create air bubbles during concrete mixing [47] and form an interface transitional zone (ITZ) [48] around the fibers. Due to the lack of adhesion [47] between the fibers and the matrix, steam can pass through. Eurocode 2 [49] currently recommends a minimum addition of 2 kg/m^3 of monofilament propylene fibers in high strength concrete mixes, and the specific properties of the fibers, such as length [45,50], diameter [24], monofilament or multifilament [50], can yield different effects. In terms of dosage, some studies suggest that higher amounts of fibers can enhance concrete permeability [43,51], reduce peak pore pressures [24,46,52], and lower the risk of spalling [12,39]. However, more PP fibers are not always better. PP fibers might reduce the compressive strength of concrete [53] and affect its flowability [54]. Longer PP fibers usually yield better results by enhancing pore connectivity and increasing the number of fibers in contact with aggregates in the ITZ [36,46]. But if the fibers are too long, such as 45 mm, their effect in reducing maximum pore pressure development is not as pronounced as that of 9 mm micro PP fibers [24]. Regarding diameter, thinner fibers improve permeability and reduce the risk of spalling under the same dosage [55], but the diameter does not significantly impact when the same quantity of fibers is used [56]. Considering multiple factors that can impact outcomes, some researchers have conducted analyses to optimize the choice of PP fibers

[14,37,39,46], considering aggregates and the granular skeleton to determine the appropriate size of PP fibers. It's evident that current research on PP fibers, from selection to mechanism studies, is quite detailed. Therefore, this report focuses on practical application experiments, aiming to simulate the conditions of tunnel liners as closely as possible to explore the role of PP fibers in spalling and the impact of the presence of PP fibers on concrete removal post-fire.

The experimental setup used in this report is derived from Maluk et al. (2016). Unlike traditional methods of temperature control in a furnace, the experiment employed a controlled radiant heat flux on concrete specimens to explore the spalling process at high temperatures. By comparing the spalling forms and temperature changes of panels, this study aims to comprehensively understand the impact of polypropylene fibers on concrete performance during and after a fire.

CHAPTER 2 EXPERIMENTAL PROGRAM

2.1. Panel Specimen

2.1.1. Concrete mix design

The size and thickness of the concrete panels are shown as shown in Figure 1. The specific parameters are as follows: the panel has a thickness of 152 mm (6 in.), a width of 457 mm (18 in.), and a height of 610 mm (24 in.). Each concrete panel was equipped with two lifting lugs at the top edge, allowing the samples to be securely transferred to the testing apparatus. To accurately monitor the internal environmental changes of the concrete, a measurement hole was drilled at the center of the bottom of each slab to measure the relative humidity inside the cured concrete. Each specimen had four k-type thermocouple sensors embedded at the center of the width and height; spaced at 25.4 mm (1 in.) on center from each other in the width direction; and located at 0 mm (0 in., e.g., surface), 6.4 mm (0.25 in.), 12.7 mm (0.5 in.), and 25.4 mm (1 in.) from the heated face. Subsequently, the exposed wires of each thermocouple were tightly twisted to facilitate connectivity [58]. At their specified depth positions, they were rotated 90 degrees to align parallel with the heating surface.

Table 1 and Table 2 summarize the properties of the steel and polypyrene fibers and the proportions and constituents used in the concrete mix design. The steel fiber concrete design is adopted from a concrete mix used in a tunnel under construction in the United States. The baseline mix utilizes Type I/II Portland cement and incorporates the following replacements by weight: 40% slag replacement and 5.33% silica fume. All of the four mixes used coarse aggregate from the same material supplier. The coarse aggregate consisted of dolomite/limestone with a saturated surface dry (SSD) specific gravity (SG) of 2.79 and absorption of 0.83%. The fine aggregate was also from the same material supplier, and had a SSD SG of 2.63. The addition of Dramix 4D steel fibers, which comply with EN 14889-1 [59] and ASTM A820-22 [60], is at a volume fraction of 0.495%. Each fiber has a length of 60 mm and a diameter of 0.75 mm, with both ends crimped to enhance adhesion to the concrete. Each fiber is composed of cold-drawn steel wire, with a nominal tensile strength of 2200 MPa, an elastic modulus of 200 GPa, and an ultimate strain of 8000 με. Polypropylene fibers with a length of 6mm from Bekaert and 19mm from Nycon were used. The specific properties of the polypropylene fibers are shown in Table 1. The four concrete mixes are defined as: SP0, no polypyrene fiber; SP2L6, which includes 2 kg/m^3 6 mm long polypyrene fiber;

SP1L6, which includes 1 kg/m^3, 6 mm long polypyrene fibers; and SP1L19, which includes 2 kg/m^3, 19 mm long polypyrene fibers.

To evaluate the compressive strength of the concrete, supplementary concrete cylinders were cast. These cylinders, with dimensions of 101.6-mm (4-in) in diameter and 203.2-mm (8-in) in height, were prepared in compliance with the ASTM C39 [61] standards. After a curing duration of 28 days, these specimens were subjected to compressive strength tests at ambient conditions. Table 2 revealed that the steel fiber-reinforced concrete exhibited a compressive strength of 66.6 MPa. This exceeds the required minimum strength of 52 MPa as dictated by the design and closely aligns with a fabricator measured value of 65.6 MPa as reported by Ouyang et al. (2023) in previous investigations.

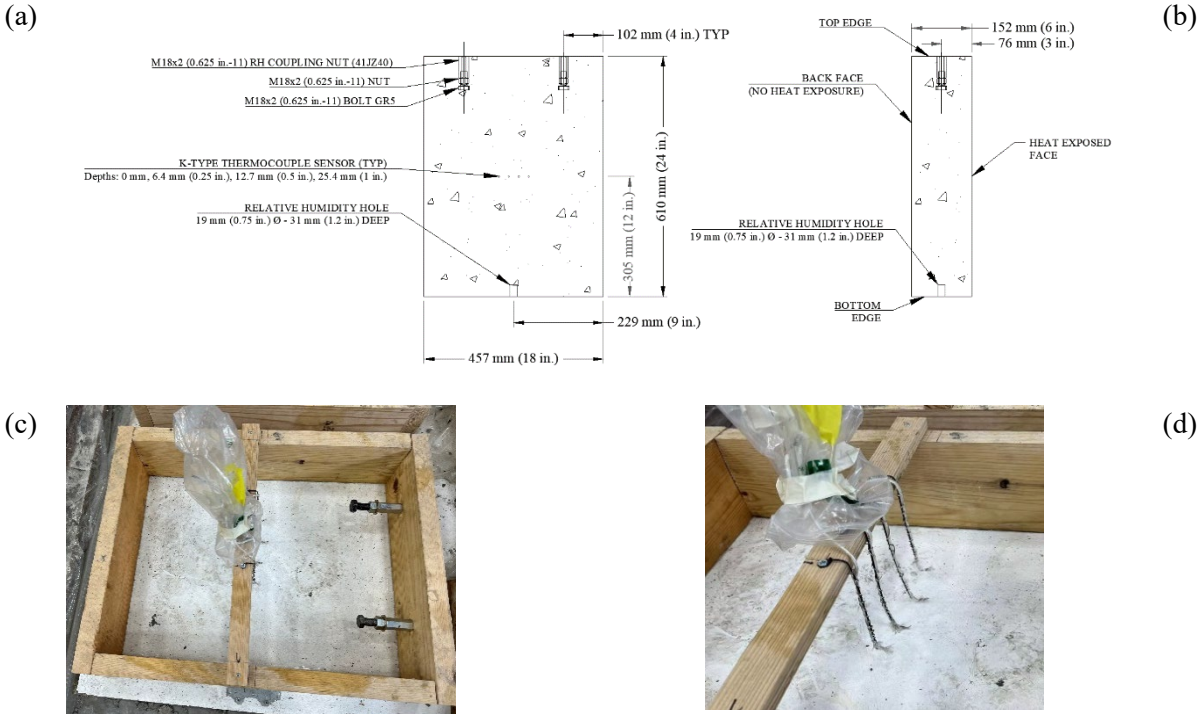

Figure 1: Concrete specimen details: (a) front view and (b) side view; (c) specimen formwork and (d) thermocouple placement for panels

Table 1: Fiber parameters

Fiber	Steel Fibers[a]	Bekaert PP Fibers[b]	Nycon PP Fibers[c]
Length [mm]	60	6	19
Diameter [mm]	0.75	0.032	0.038
Tensile Strength [MPa]	2200	300	17
[a] https://www.bekaert.com/en/product-catalog/content/dop/dramix-4d-technical-documents			

[b] https://www.bekaert.com/en/product-catalog/content/dop/duomix-ce-documents
[c] https://nycon.com/products/procon-m

Table 2: Summary of concrete mix design and thermo-mechanical properties

Mix	SP0	SP2L6	SP1L6	SP1L19
Type I Cement [kg/m^3]	243.4	242.9	243.1	243.1
Grade 120 GBFS [kg/m^3]	175.7	175.3	175.5	175.5
Sikacrete 950 DP Silica Fume [kg/m^3]	24.0	23.9	23.9	23.9
Free Water [kg/m^3]	151.1	150.8	151.0	151.0
Water/Cement Ratio	0.35	0.35	0.35	0.35
#8 Coarse Aggregate SSD [kg/m^3]	1018.0	1015.8	1016.9	1016.9
Coarse Aggregate Type	Dolomite /Limestone			
ASTM C33 Fine Aggregate SSD [kg/m^3]	698.6	696.0	696.8	696.8
Air Entraining Admixture (Daravair 1000) [mL/m^3]	228.7	228.6	228.5	228.5
High Range Water Reducer (EXP 950) [mL/m^3]	1095.2	1094.6	1093.4	1093.4
Design Air (entrained)	6%	6%	6%	6%
Steel Fiber (Dramix 4D Fiber) [kg/m^3]	38.6	38.6	38.6	38.6
Steel Fiber Volume Ratio	0.495%	0.495%	0.495%	0.495%
Polypropylene Fiber (monofilament) [kg/m^3]	0	2	1	1
Polypropylene Fiber Volume Ratio	0%	0.220%	0.110%	0.110%
Polypropylene Fiber Length [mm] (Supplier)		6 (Bekaert)	6 (Bekaert)	19 (Nycon)
Measured Slump [mm]	38.1	28.6	31.1	25.4
Measured Wet Unit Weight [kg/m^3]	2440.7	2404.3	Not measured	Not measured
Average Compressive Strength [MPa] (28 days)	66.6±3.3	56.3±2.0	61.7±1.4	70.9±4.9
Thermal Conductivity [W/m-K]	3.267	2.813	3.014	3.176
Thermal Diffusivity [mm^2/s]	1.29	1.33	1.27	1.31
Specific Heat [MJ/m^3-K]	2.528	2.122	2.379	2.427

(a) (b) (c)

Figure 2: Fibers (a) steel fibers, (b) Bekaert PP fibers, and (c) Nycon PP fibers

Thermal properties of the concrete were characterized under ambient conditions following the guidelines laid out by ISO 22007-2 [63], utilizing a Hot Disk TPS 2500S [64] system. For these

measurements, a 4921 F1 Mica sensor with a diameter of 9.7 mm was positioned between two untested concrete disc samples, each having a thickness of 25.4 mm (1 in.). The concrete samples were extracted from cylindrical specimens. The TPS 2500S system enabled direct determination of the thermal conductivity, k (W/m-K), and diffusivity, D (mm^2/s). Subsequent calculations were performed to deduce the volumetric heat capacity, s (MJ/m^3-K), which was reported on a volumetric basis, in alignment with ISO 22007-2 [63]. The specific heat capacity or heat capacity per unit mass, c_p (MJ/kg-K), was ascertained using the dry stacked bulk density, ρ (kg/m^3), as determined by ASTM C642-13 [65]. Comprehensive thermal analyses were conducted at varying temperatures: ambient, 100°C, 200°C, 280°C, 420°C, and 500°C. The thermal outcomes at elevated temperatures will be elucidated in the subsequent section.

$$s = \frac{k}{D} = \rho \cdot c_p \tag{1}$$

2.1.2. Pre-test specimen conditions

Prior to thermal experimental assessment of each concrete panel, moisture content, relative humidity, and ambient temperature were measured using the Tramex CMES Digital Moisture Meter [66]. All measurements were taken within 4 hrs. of each panel test. This digital hygrometer determines moisture levels within the outer 19 mm (0.75 in.) layer of the panel surface via resistive impedance, presenting results in terms of percentage of solid mass. Moisture content readings were taken at nine points on the heated face, and were averaged. Following the ASTM F2170 [67] guidelines, relative humidity was gauged using a hygrometer probe inserted into a 30.5-mm (1.2 in) deep hole at the bottom of the concrete panel, as illustrated in Figure 1.

Table 3: Summary of pre-test panel specimen conditions

Specimen Label	Test Age [day]	MC [%]	Air Temp. [°C]	Sat. Vapor Density [g/m^3]	RH [%]
SP0-1	77	4.6±0.2	24.5	12	66.7
SP0-2	80	4.8±0.3	24.6	13	67.9
SP2L6-1	83	5.1±0.1	27.2	14	65.7
SP2L6-2	84	5.0±0.2	27.9	16	70.6
SP1L6-1	83	4.9±0.4	28.1	16	67.1
SP1L6-2	84	4.7±0.2	25.4	13	65.9
SP1L19-1	88	4.3±0.4	22.1	10	62.9
SP1L19-2	89	4.4±0.2	21.6	9	61.1

The panels underwent a seven-day curing process under wet burlap and were subsequently left to air cure. Table 3 provides a comprehensive summary of the pre-test conditions of the concrete panels. The relative humidity of all samples remained below the 75% threshold stipulated by ASTM E119 [68]. Additionally, moisture content for all slabs consistently ranged between 4.0% and 5.0%. This is comparative to typical moisture levels encountered in tunnel linings [69].

2.2. Test Setup

The testing apparatus consists of a self-reacting loading frame and heating source mounted on a movable track to control heat flux delivery as shown in Figure 3. A self-reacting load frame with two through-hole hydraulic actuators delivered axial load to the concrete specimen with the heating source mounted on a separate track. The testing apparatus was designed to allow for variation in applied axial load in one-direction while providing variation in applied thermal loading via standoff distance between the heat source and specimen.

Figure 3: Concrete heat and loading frame

The self-reacting frame consists of two double webbed, built-up I-sections acting as spreader beams to distribute the loading frame and specimen weight over a larger floor area. Between the spreader beams dual webs, an opening was cut to facilitate access to, and placement of, the capping nut and washers for the threaded rod and load cells. The threaded rod's bottom nut and washer sandwiches the hollow pipe-style load cell between the washer and the bottom of the spreader beam's top flange. The threaded rod passes through a hollow section hydraulic actuator ram and

through a welded plate and the wide flange section that acts as the base support for the concrete specimen. The threaded rods pass along the sides of the concrete specimen and through the top built-up plate and wide flange section that acts as the top support for the concrete specimen, and are capped at the top with a nut and washer. The configuration allows for the hydraulic rams to push the bottom specimen support beam upward compressing the concrete sample against the top support beam.

The hydraulic actuators are controlled via a pressure regulated hydraulic pump. The in-line load cells are used to verify the delivered axial load as well as monitor the variation throughout the heat exposure duration. Axial load of 600 kips can be applied, accommodating up to 30% of the compressive strength of the concrete panel.

The heat source support frame allows for three-dimensional adjustment of the heat source. A sled and track system, which allows movement of the heat source in the direction normal to the exposed specimen surface, was integrated into the heat source support frame. Rapid standoff closing was needed to reduce the effect of heat source ignition on the sample before the initiation of the calibrated heat flux curve, while also adding an element of safety during ignition with increases standoff between specimen and heater.

Figure 4 shows the axial and heat loading frame setup; note the inclusion of insulation wrapping for the heat exposed threaded rod and the hydraulic actuator rams, a spall fragment protection screen, and labeling showing thermocouple sensors. The spall fragment protection screen was constructed of a welded carbon steel angle frame with two layers of stainless-steel welded wire mesh bolted in-place at 101.6 mm (4 in.) bolt to bolt spacing around the steel angle frame perimeter. The stainless-steel mesh layers were replaced after every 40 minutes of heat exposure. Several heat exposure cycle iterations were evaluated during heat flux calibration to set the mesh replacement schedule such that the presented heat flux curves were minimally affected by screen condition. The protection screen does impede heat flux delivery to the specimen surface, however all calibration curves presented were recorded with the screen in place (heat flux calibration is discussed in more depth in the next section). Three to four thermocouple sensors were embedded within the concrete specimens at staggered distances from the heat exposed specimen face. Additionally, two thermocouple sensors were placed in contact with the specimen at the top and bottom of the heat exposed area, located on center of the specimen width, between the spall

protection screen and specimen. The surface temperatures reported, herein, are the top and bottom surface measurements average.

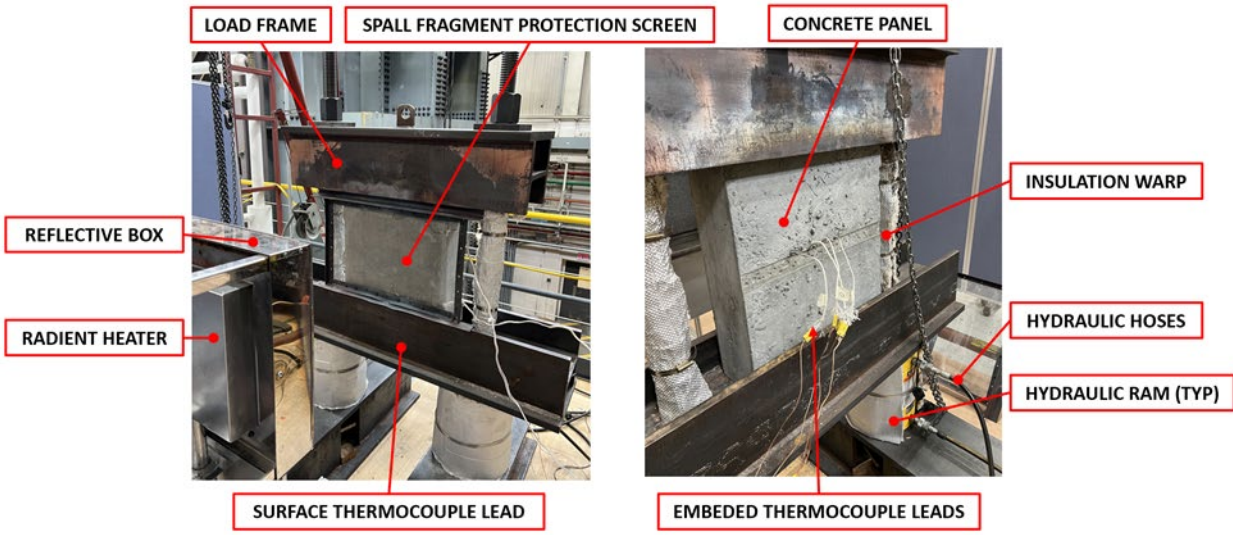

(a) Front view (b) Rear view

Figure 4: Self-reacting axial and heating load frame

Surface thermocouples were placed at the specimen width centerline, located at the top and bottom of the heat exposed specimen area. The heater was ignited at a distance of 686 mm (27 in) and rapidly moved to the testing distance of 152 mm (6 in) from the concrete specimen.

For this test program, each panel was initially loaded with a target of 20% (10.34 MPa) of the design strength, specifically 51.71 MPa (7500 psi), multiplied by the total cross-sectional area. The target stress level represents the in-situ stress present in typical tunnel lining systems. The thermal load was applied to one face of the specimen as radiant heat flux by adjusting the spacing distance between the radiating plate and the specimen. The radiating plate surface is composed of a metallic mesh fixed on a peripheral frame, and a reflector box surrounds it to produce consistent thermal exposure to the specimen.

A fragmentation protection screen was inserted in front of the samples between the secondary beams to prevent damage to the radiating plate. This screen is made up of two layers of stainless-steel welding wire with 6.4 mm (0.25 inches) square openings, bolted onto a welded steel angle peripheral frame. Due to the permanent bending caused by high-intensity heating and potential spalling fragment impacts, the stainless-steel mesh layer was replaced after each test on the two panels with steel fibers only. For the remaining panels with added PP fibers, the stainless-steel mesh layer was replaced after every two panels. During the calibration prior to the official testing,

the heat flux transferred to the sensors showed minimal variation during the initial two heating cycles (one hour each) with the same stainless-steel mesh layer, which will be elaborated on in the next section.

During each experimental run, the radiation board was activated at a predetermined distance of 686 mm (27 in.) from the sample heating surface. Calibration conducted prior to the primary tests confirmed that at this distance, the heat flux applied to the sample remained below 6 kW/m^2. After ignition, upon reaching a stable state in approximately 20 seconds, the radiation board connected to the vertical support frame was promptly repositioned to the anticipated isolation distance, a process that took no more than 10 seconds.

2.3. Thermal Exposure

In the realm of fire safety studies, the exposure of heat flux from radiation heaters aims to emulate, as closely as possible, within the constraints of the apparatus, the high-level near-field thermal exposures observed in tunnel hydrocarbon fires or vehicular conflagrations. Notably, standards such as NFPA502 [70] and RABT prescribe temperature-time histories for confined spaces, where temperatures escalate rapidly to near-peak exposures, typically within a span of no more than 5 minutes. The experimental apparatus utilizes real-time heat flux as the controlling variable. Leveraging the first principles of heat transfer in conjunction with semi-empirical data, it becomes feasible to approximate the temperature-time trajectory of standard fire curves, such as those delineated in the hydrocarbon standard fire curve of ASTM E1529-16 [71], into an equivalent applied heat flux-time trajectory. The ASTM E1529-16 stipulates direct equivalent metrics for the development of fire resistance ratings for structural elements and mechanical components: either a constant temperature exposure of 1095±85°C or an equivalent constant heat flux of 158±8 kW/m^2, with both metrics needing attainment within the initial 5 minutes. This curve presents an apt approximation for typical vehicular and cargo fires within tunnels according to Guo's research [72]. As such, our testing apparatus has been benchmarked against the heat flux exposures outlined in ASTM E1529 [71].

Figure 5 illustrates the gas-fired radiant panel prepared for this experiment. The entire system comprises a blower optimized for fuel-to-air ratio, an electrical controller for fuel mixing and ignition, and an elevated rectangular fuel supply box topped with 304.8 millimeters (12 inches). Natural gas is supplied at a constant flow rate through perforated pipes behind the panel. When

the gas combusts in a stable state, its metallic material becomes incandescent and radiates. Concurrently, reflector boxes are installed around the radiation panel, aimed at mitigating the rising airstream and assisting in focusing the radiant heat flux onto the sample.

In this experiment, the incident heat flux transmitted to the sample surface was measured using a water-cooled Hukseflux SBG01 radiometer [73]. The measurement of heat flux was conducted prior to heating the concrete slab sample, as depicted in Figure 5. To ensure the accuracy of the measurements, a protective screen was also added in front of the radiometer. Concurrently, it was flush mounted through the center hole of 19.1 mm (0.75 in.) thick steel plate, the dimensions of which were the same as the surface of the concrete slab sample: 457.2 mm (18 in.) in width × 609.6 mm (24 in.) in height. The interval between two measurements exceeded 4 hours to ensure that the initial heat flux was sufficiently minimal.

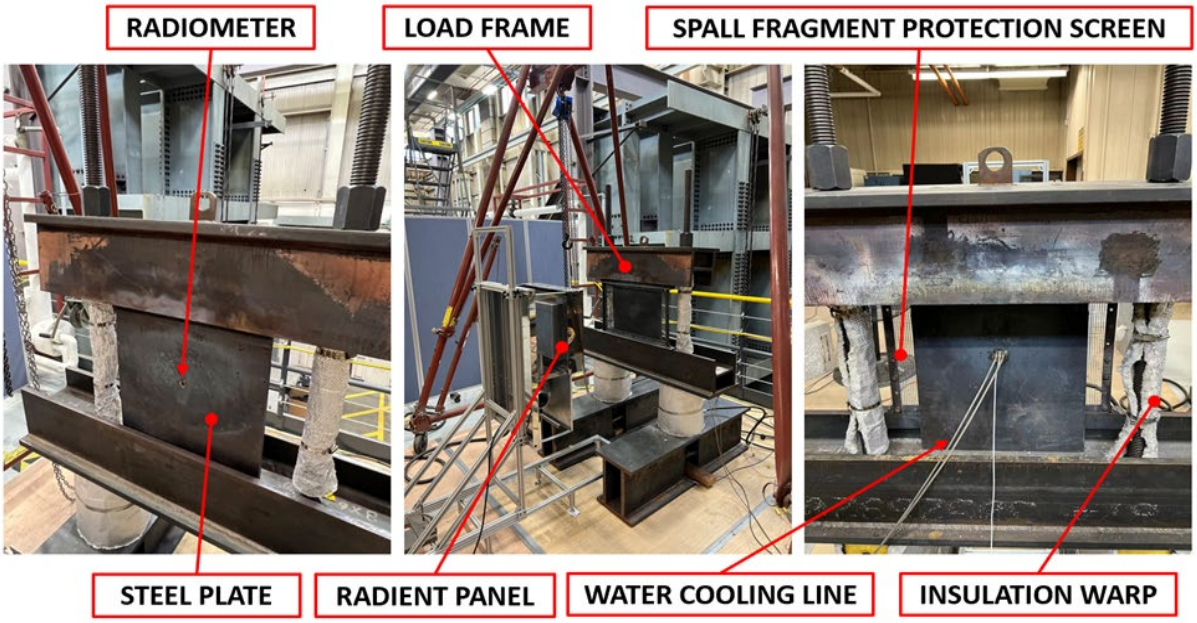

(a) Front view (b) Front view w/screen (c) Rear view

Figure 5: Testing apparatus heat flux calibration setup

Pre-test measurements were completed within 1 hour of thermal exposure. After prolonged combustion, the upper flange of the reflector box exhibited warping and perforations, as shown in Figure 6. Consequently, a replacement was carried out during the calibration phase, and the heat flux variations over time were re-measured. The results shown in the Figure 7 include average heat flux time history before the replacement of the top flange and a comparison with average heat flux time history after the top flange was changed. In the first 3 minutes, before the top flange was replaced, the heat flux increased faster. After 15 minutes, when the heat flux stabilized, the heat

flux was slightly lower than the heat flux after the top flange was replaced, but the overall difference was smaller. In the interval from 15 minutes to 60 minutes before and after replacement, the heat flux remains basically stable. Thus, in the experiments involving all eight concrete panels, it can be inferred that the input heat flux across each slab remained relatively consistent. Within the initial 5 minutes of heating, the heat flux reaches approximately 140 kW/m^2, which is roughly 89% of the value stipulated by ASTM E1529 [71]. By the 15-minute mark, the heat flux ascends to 150 to 158 kW/m^2 and sustains this level until the 60-minute interval. Table 4 presents the average heat flux observed in two distinct intervals: the initial 60 minutes and the period from 5 to 60 minutes. Following the replacement of the top flange, the average heat flux recorded between 5 to 60 minutes was 156.1 kW/m², closely aligning with the value of 158 kW/m².

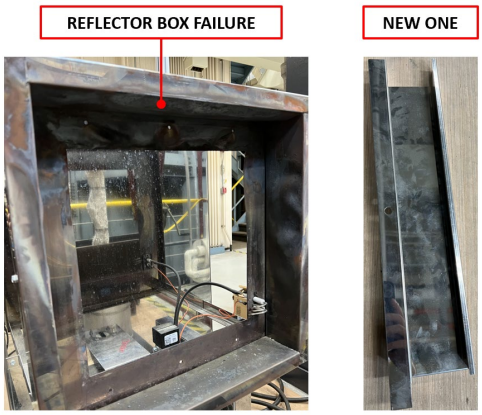

Figure 6: Reflector box

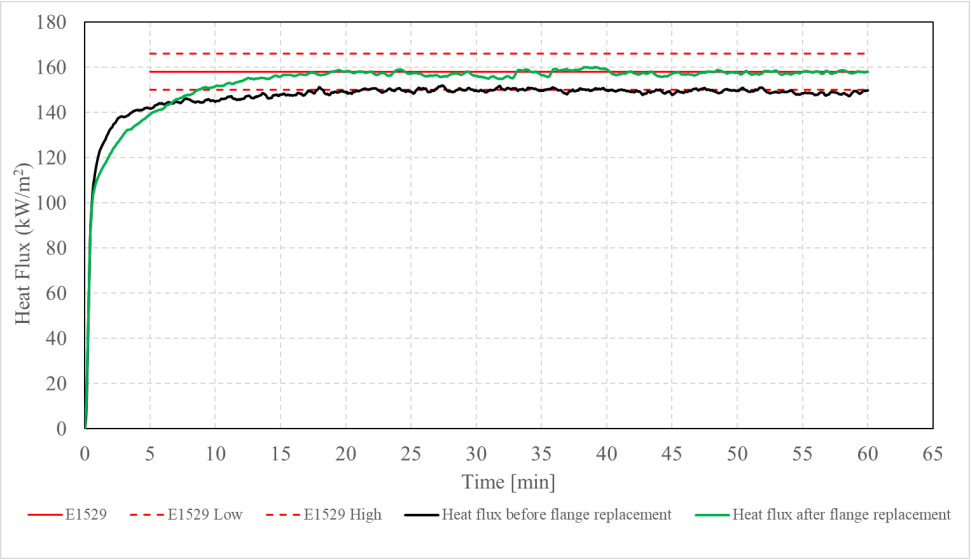

Figure 7: Radiant heat flux calibration for different radiant panel face configurations and ASTM E1529 hydrocarbon fire values

Table 4: Average heat flux

Average heat flux (kW/m^2)	From 0 to 60 min	From 5 to 60 min
Before flange replacement	146.7	148.8
After flange replacement	152.9	156.1

The spatial distribution of the heat flux was explored, as depicted in Figure 8. For these measurements, the compact and portable FluxTeq HTHFS-01 heat flux sensor [74] was employed. The sensor has a thickness of 3 millimeters and was positioned in direct contact with the frontal surface of the steel plate. A total of 12 distinct locations were evaluated in 12 separate heating tests (as shown in Figure 8, black points). The primary variation in each assessment was the positioning of the heat flux sensor. For each measurement at each point, the heating time was set to 1h. The data between the 19.5-minute and 20-minute marks were averaged to obtain the value of the heat flux for that point. Using this method, the heat flux values for 12 individual measurement points were obtained. Subsequently, these values were normalized against the measurement obtained at the central position for comparative analysis. Figure 8 presents the heat flux percentage contour based on the measurements from 12 points (The assumption is made that the lateral heat flux decay is symmetric about the panel centerline). From Figure 8, two distinct trends can be discerned: firstly, a progressive increment in heat flux is evident as one transitions from the bottom to the top of the heated region; secondly, a decay in heat flux manifests as one moves from the center towards the periphery. The former trend can be attributed to the upward movement of the hot gases produced by the combustion of natural gas. These gases are impeded by the upper flange edge of the reflector box, resulting in heat accumulation at the top. The latter trend arises due to the reflective enclosure surrounding the radiative panel, which effectively redirects the thermal exposure back to the central portion of the specimen's surface.

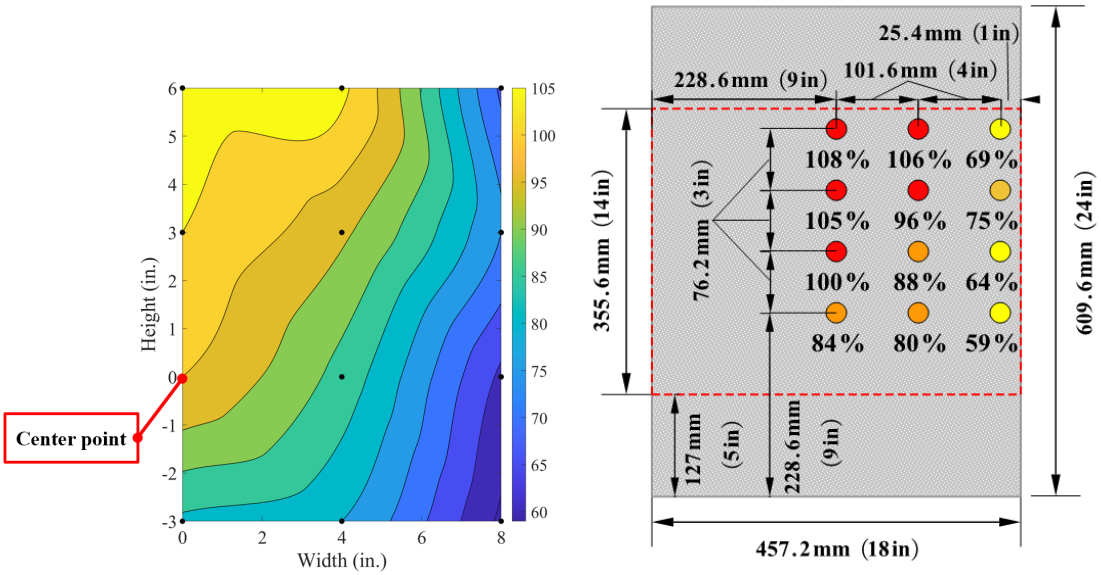

Figure 8: Heat flux contour [%] and discrete measurements

2.4. Applied Axial Loading

Figure 9 illustrates the time history of the total axial load exerted by two hydraulic cylinders during the first 5 minutes and first 50 minutes of exposure. The panels that experienced spalling are represented by grey lines, while those that did not spall are depicted with black lines. Notably, the SP0-2 panel data were processed using a moving average method. Each specimen's initial load was within ±5% of the target load and did not increase more than 19% from the initial value. It was observed that, within the first 5 minutes (and until the end of heating for panels with only steel fibers), there was an increase in the load values. This rise is attributed to the uneven thermal expansion of the panel thickness and the simplicity of the loading setup. The increase in load during the first 5 minutes was roughly the same across the samples, as depicted in the Figure 9 (a). For the spalling panels, the peak load values were reached right up to the point of spalling. During the 20 to 25-minute interval of the heating process, the non-spalling panels in the study reached their maximum load values. This suggests that the structural integrity of these samples was maintained up to this point, despite the thermal stress. After reaching these peak values, the load gradually decreased, indicating a possible relaxation or adjustment in the material due to prolonged exposure to heat. According to Table 5, the maximum stress change in the load did not exceed 4% of the design compressive strength.

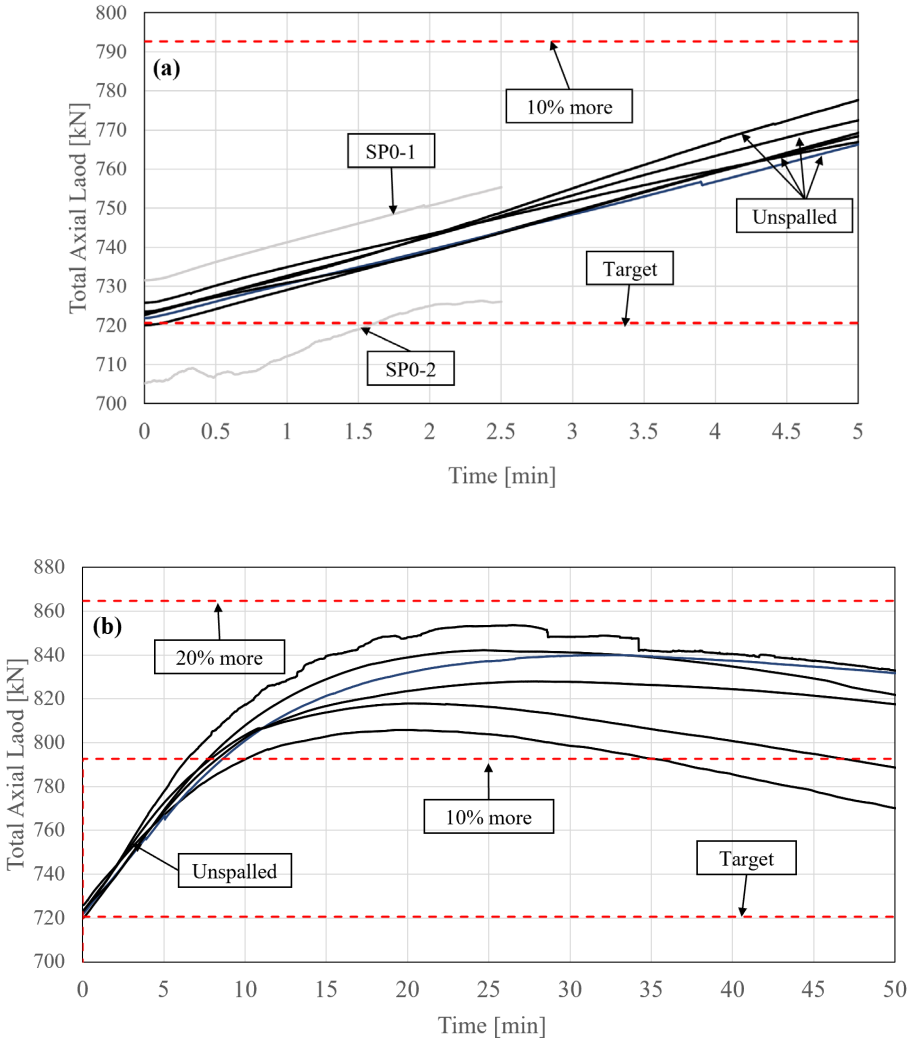

Figure 9: Axial load history during each test: (a) first 5 min, and (b) up to 50 min.

CHAPTER 3 RESULTS AND DISCUSSION

Table 5 provides a comprehensive summary of the testing outcomes for all the samples. Figure 10 shows water seepage from the side of panel during heating. Figure 11-Figure 14 illustrate photos of each panel before heating, the day after heating, and two months (except for the panels without PP fibers) after being placed in air for panels without experiencing spalling. In the two panels without added polypropylene fibers, complete spalling occurred, and due to the intense nature of the spall process, heating was terminated approximately after around 2.5 minutes, commencing the timing once the radiant panel was ignited and positioned 6 in. from the specimen face. After this, the radiant panel was turned off and safely retracted along the sled track. For the other six panels with polypropylene fibers, heating was continuously maintained for around 1 hour to simulate the prolonged fire exposure effects on concrete. In the initial 10 minutes of heating, liquid water (Figure 10) could be observed on the sides of the concrete panels, particularly in the upper-middle region, due to higher heat flux in that area.

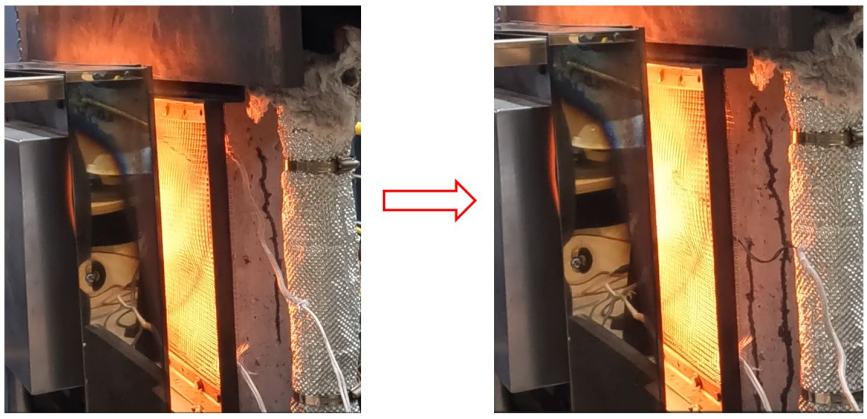

Figure 10: Water seepage on concrete panel during heat exposure

3.1. Panel Test

The onset of spalling for SP0-1 and SP0-2 was recorded at 107 seconds and 109 seconds, respectively, accompanied by an audible 'bang', at which point a substantial volume of fragments and larger pieces were propelled into the protective screen. Throughout the heating period, each panel underwent two major spalling events, with numerous minor instances of spalling occurring before and after the major event, manifested as a 'pitter-patter' sound. The moisture content (MC) in both panels exceeded 4%, significantly surpassing the safety threshold established in prior experiments by Carlton [58]. Although the steel fibers provide a bridging effect [75] that helps to

maintain the structural integrity of the concrete and control crack propagation, their presence alone was not sufficient to prevent spalling in this study.

SP0-1 before heating | SP0-1 after heating | SP0-2 before heating | SP0-2 after heating

Figure 11: Panels without polypropylene fibers (SP0)

Table 5: Summary of heated panel test results.

Label	Applied Axial Stress [% of 7500 psi]		Explosive Spalling Event	End of Heating [min]	Spall Time [min]	Max. Spall Depth [mm]
	Avg.	Max.				
SP0-1	20.38	20.96	Y	2.5	1.78	9.8
SP0-2	19.87	20.16	Y	2.5	1.82	9.4
SP2L6-1	22.47	23.38	N	60	No spall	
SP2L6-2	21.45	22.32	N	60		
SP1L6-1	22.72	23.69	N	60		
SP1L6-2	22.39	23.31	N	54		
SP1L19-1	22.25	22.98	N	60		
SP1L19-2	21.84	22.70	N	60		

Figure 12 to Figure 14 illustrate that among the six concrete panels reinforced with polypropylene fibers, the two panels with an addition of 1 kg/m³ of 19 mm long fibers exhibited the best performance. These panels only exhibited a change in the concrete surface color to a grey reddish hue with visible cracks forming on the surface, yet no spalling occurred throughout the heating process. The two panels with 2 kg/m³ of 6 mm long fibers, while displaying a similar discoloration, experienced minor spalling in small localized areas with shallow depth and were accompanied by a faint 'pitter-patter' sound at the onset of heating. In contrast, panel SP1L6-1, with 1 kg/m³ of 6 mm long fibers, exhibited more extensive early-stage spalling compared to those with 2 kg/m³ of polypropylene fibers. This panel also showed the most severe peeling on the concrete surface, with a substantial number of cracks forming.

After being exposed to the laboratory environment for a period ranging from 46 to 61 days, all the fire exposed panels with PP fibers exhibited additional widespread surface delamination. The extent of this delamination did not show a significant pattern correlating with the content or size of the PP fibers used. This phenomenon aligns with the post-cooling spall. This type of spalling typically occurs in concrete with calcareous aggregates. Upon cooling, the calcium oxide on the surface reacts with moisture in the air to form calcium hydroxide, causing expansion and significant internal microcracking. This process leads to the complete loss of concrete strength and results in the gradual flaking off of the surface after cooling.

SP2L6-1

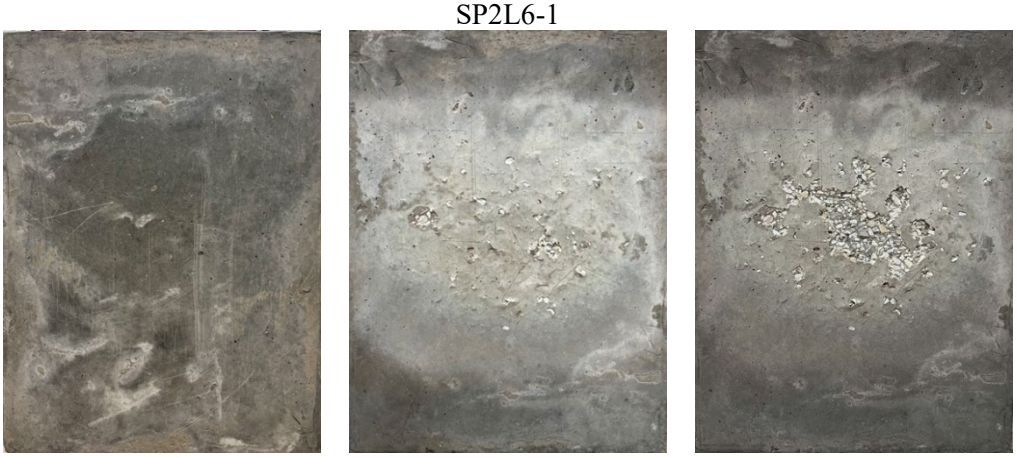

before heating | 1 day after heating | 61 days after heating

SP2L6-2

before heating | 1 day after heating | 60 days after heating

Figure 12: Panels with 2kg/m^2, 6mm long polypropylene fibers (SP2L6)

SP1L6-1

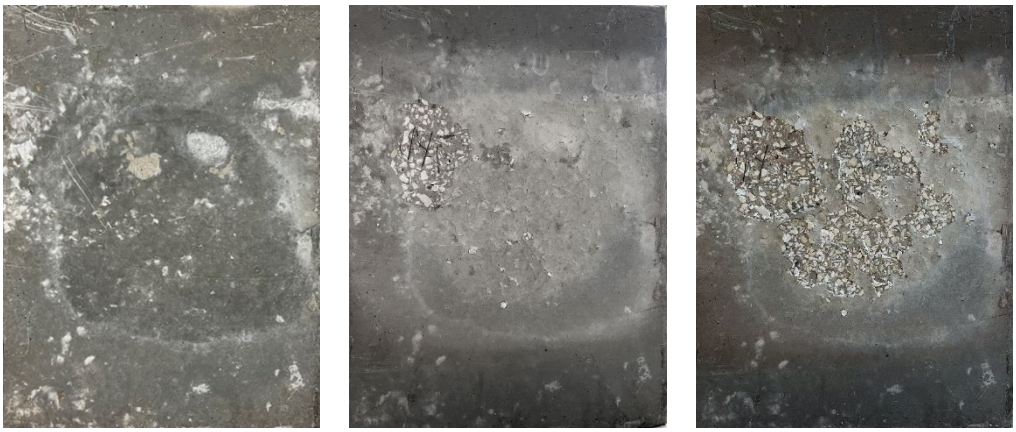

before heating 1 day after heating 56 days after heating

SP1L6-2

before heating 1 day after heating 55 days after heating

Figure 13: Panels with 1kg/m^2, 6mm long polypropylene fibers (SP1L6)

3.2. Temperature Time History

Figure 15 presents the temperature change within the concrete panels. It's important to note that the thermocouples placed at a depth of 25.4 mm were largely malfunctioning, and as a result, Figure 15 does not include temperature curves measured by thermocouples at this depth. For the thermocouples at the other three depths, some were either non-functional before the measurement started or experienced temporary malfunctions during the measuring period. Therefore, Figure 15 shows the temperature curves recorded by the thermocouples when they were functioning correctly.

Figure 15 reveals that throughout the heating process, the surface temperature changes were broadly similar in value. This similarity is attributed to the fact that the only differences in their mixtures were the content and length of the polypropylene fibers, while their thermal properties remained relatively consistent. As the depth increased, the disparity between the curves became more pronounced. However, the temperature time histories within the panels during the initial phase of heating were still very close, showing good consistency. This consistency allows for a

valid comparison with results from numerical simulations, aiding in obtaining more accurate temperature change curves. The initial thermal gradients in the panels were not significantly different due to the uniformity of temperature changes at the beginning of the heating process. The key factor determining whether a panel would spall was the magnitude of internal pore pressure and the ability to promptly relieve this pressure. The results suggest that adding more and longer polypropylene fibers is beneficial for the release of pore pressure, a finding that aligns with results obtained by Shen et al. [46] and Bangi and Horiguchi [28].

Figure 16 illustrates the change in surface temperature during the first 3 minutes. Due to the higher thermal conductivity of steel fiber-reinforced concrete, the initial temperature rise is faster compared to concrete with added polypropylene fibers.

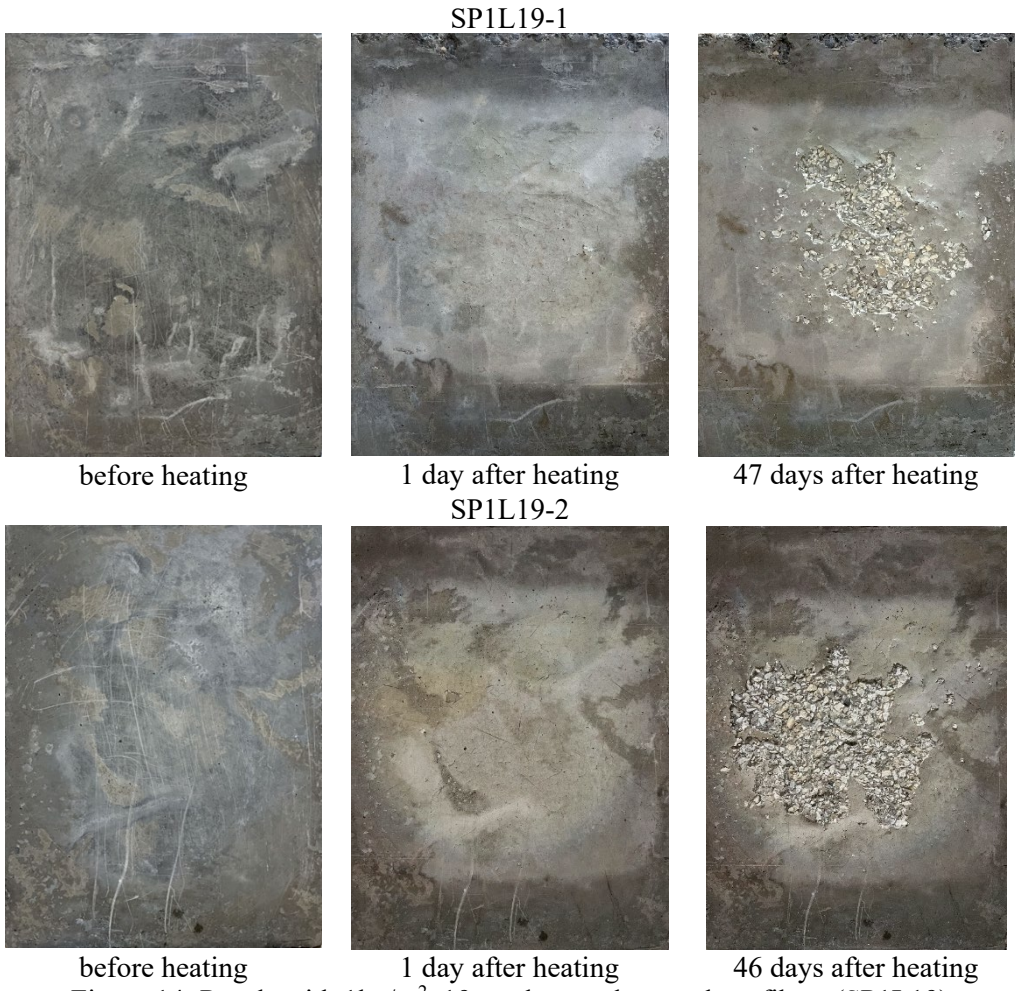

Figure 14: Panels with 1kg/m^2, 19mm long polypropylene fibers (SP1L19)

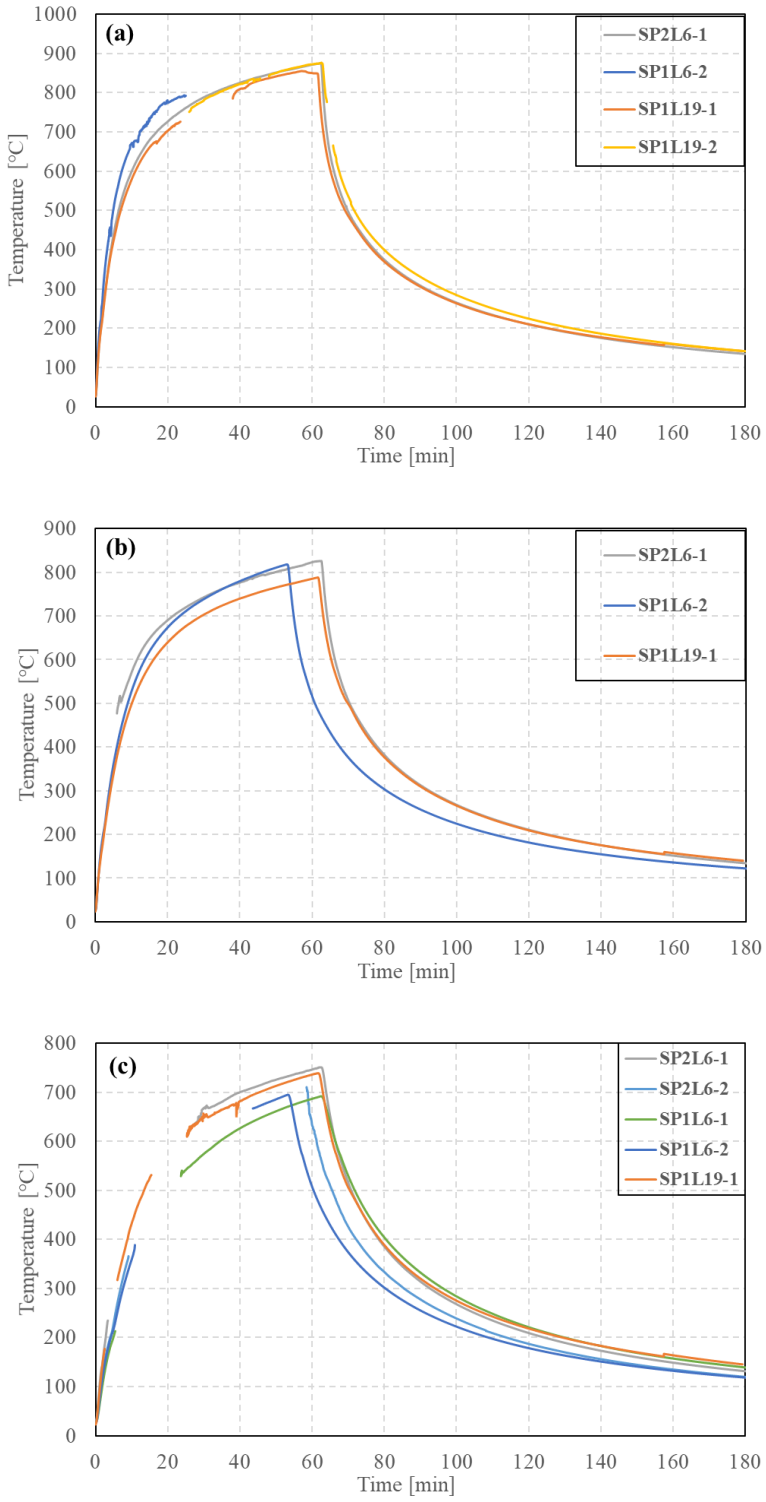

Figure 15: Temperature history recorded through the thicknesses of each specimen: (a) surface, (b) 6.4mm and (c) 12.7mm

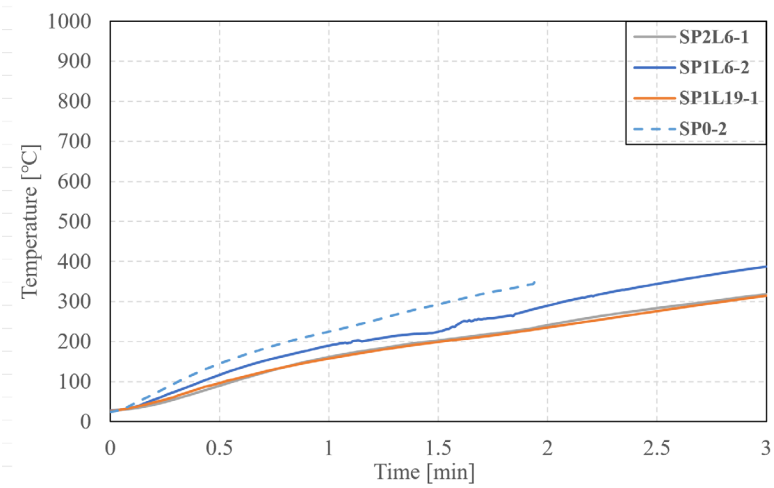

Figure 16: Surface temperature during the first 3 minutes of heating

CHAPTER 4 CONCLUSION

A comprehensive performance evaluation of concrete with added polypropylene fibers in comparison to concrete without polypropylene fibers under exposure to representative hydrocarbon/vehicle fires was conducted in this study. Experiments demonstrated that the inclusion of polypropylene fibers in concrete significantly reduces the propensity for spalling when subjected to fire conditions. Concrete specimens containing only steel fibers exhibited spalling before reaching a moisture content of 4% to 5%, with spalling initiating within the first two minutes of heating. This spalling phenomenon progressed layer by layer.

The impact of polypropylene fiber content and length on spalling control was pronounced. When utilizing 1 kg/m³ of 6mm length polypropylene fibers, the surface layer of concrete still experienced very shallow spalling. However, as the length and content of polypropylene fibers increased, spalling was entirely prevented throughout the entire 1-hour heating cycle.

It is worth noting that post-cooling damage, which occurs after the concrete has been exposed to heat and subsequently cooled, was observed. It is hypothesized that this is due to the presence of calcium aggregates used in the concrete mix. Unfortunately, polypropylene fibers alone were unable to entirely eliminate this post-cooling spalling phenomenon.

REFERENCES

[1] Sakkas K, Vagiokas N, Tsiamouras K, Mandalozis D, Benardos A, Nomikos P. In-situ fire test to assess tunnel lining fire resistance. Tunn Undergr Space Technol 2019;85:368–74. https://doi.org/10.1016/j.tust.2019.01.002.

[2] Lee WM, Fragomeni S, Monckton H, Guerrieri M. A review of test Methods, issues and challenges of Large-Scale fire testing of concrete tunnel linings. Constr Build Mater 2023;392:131901. https://doi.org/10.1016/j.conbuildmat.2023.131901.

[3] Sideris KK, Manita P. Residual mechanical characteristics and spalling resistance of fiber reinforced self-compacting concretes exposed to elevated temperatures. Constr Build Mater 2013;41:296–302. https://doi.org/10.1016/j.conbuildmat.2012.11.093.

[4] Zhang P, Kang L, Wang J, Guo J, Hu S, Ling Y. Mechanical Properties and Explosive Spalling Behavior of Steel-Fiber-Reinforced Concrete Exposed to High Temperature—A Review. Appl Sci 2020;10:2324. https://doi.org/10.3390/app10072324.

[5] Ma Q, Guo R, Zhao Z, Lin Z, He K. Mechanical properties of concrete at high temperature—A review. Constr Build Mater 2015;93:371–83. https://doi.org/10.1016/j.conbuildmat.2015.05.131.

[6] Amran M, Huang S-S, Onaizi AM, Murali G, Abdelgader HS. Fire spalling behavior of high-strength concrete: A critical review. Constr Build Mater 2022;341:127902. https://doi.org/10.1016/j.conbuildmat.2022.127902.

[7] Bisby L, Mostafaei H, Pimienta P. White paper on fire resistance of concrete structures. Gaithersburg, MD: National Institute of Standards and Technology; 2014. https://doi.org/10.6028/NIST.GCR.15-983.

[8] Noumowe A, Carre H, Daoud A, Toutanji H. High-Strength Self-Compacting Concrete Exposed to Fire Test. Jounal Mater Civ Eng 2006;18:754–8. https://doi.org/10.1061/(ASCE)0899-1561(2006)18:6(754).

[9] Phanl LT. Effects of elevated temperature exposure on heating characteristics, spailing, and residual properties of high performance concrete n.d.

[10] Choe G, Kim G, Yoon M, Hwang E, Nam J, Guncunski N. Effect of moisture migration and water vapor pressure build-up with the heating rate on concrete spalling type. Cem Concr Res 2019;116:1–10. https://doi.org/10.1016/j.cemconres.2018.10.021.

[11] Carvel RO, Beard AN, Jowitt PW, Drysdale DD. Fire Size and Fire Spread in Tunnels with Longitudinal Ventilation Systems. J Fire Sci 2005;23:485–518. https://doi.org/10.1177/0734904105052578.

[12] Li Y, Tan KH, Yang E-H. Synergistic effects of hybrid polypropylene and steel fibers on explosive spalling prevention of ultra-high performance concrete at elevated temperature. Cem Concr Compos 2019;96:174–81. https://doi.org/10.1016/j.cemconcomp.2018.11.009.

[13] Polanczyk A, Majder-Lopatka M, Dmochowska A, Salamonowicz Z. Analysis of Combustion Process of Protective Coating Paints. Sustainability 2020;12:4008. https://doi.org/10.3390/su12104008.

[14] Sultangaliyeva F, Fernandes B, Carré H, La Borderie C. Optimizing choice of polypropylene fiber geometry for preventing spalling of high performance concrete due to fire. Fire Saf J 2023;136:103759. https://doi.org/10.1016/j.firesaf.2023.103759.

[15] Marcos-Meson V, Michel A, Solgaard A, Fischer G, Edvardsen C, Skovhus TL. Corrosion resistance of steel fibre reinforced concrete - A literature review. Cem Concr Res 2018;103:1–20. https://doi.org/10.1016/j.cemconres.2017.05.016.

[16] di Prisco M, Plizzari GA. Precast SFRC elements: From material properties to structural applications. 6th Int. RILEM Symp. Fibre Reinf. Concr., RILEM Publications SARL; 2004, p. 81–100.
[17] Serna P, Arango S, Ribeiro T, Núñez AM, Garcia-Taengua E. Structural cast-in-place SFRC: technology, control criteria and recent applications in spain. Mater Struct 2009;42:1233–46. https://doi.org/10.1617/s11527-009-9540-9.
[18] de Waal RGA. Steel fibre reinforced tunnel segments-for the application in shield driven tunnel linings 2000.
[19] Abbas S. Structural and durability performance of precast segmental tunnel linings. The University of Western Ontario (Canada); 2014.
[20] Plizzari GA, Tiberti G. Steel fibers as reinforcement for precast tunnel segments. Saf Undergr Space - Proc ITA-AITES 2006 World Tunn Congr 32nd ITA Gen Assem 2006;21:438–9. https://doi.org/10.1016/j.tust.2005.12.079.
[21] Aydın S, Yazıcı H, Baradan B. High temperature resistance of normal strength and autoclaved high strength mortars incorporated polypropylene and steel fibers. Constr Build Mater 2008;22:504–12. https://doi.org/10.1016/j.conbuildmat.2006.11.003.
[22] Khoury GA. Effect of fire on concrete and concrete structures. Prog Struct Eng Mater 2000;2:429–47. https://doi.org/10.1002/pse.51.
[23] Peng G-F, Yang W-W, Zhao J, Liu Y-F, Bian S-H, Zhao L-H. Explosive spalling and residual mechanical properties of fiber-toughened high-performance concrete subjected to high temperatures. Cem Concr Res 2006;36:723–7. https://doi.org/10.1016/j.cemconres.2005.12.014.
[24] Ding Y, Zhang C, Cao M, Zhang Y, Azevedo C. Influence of different fibers on the change of pore pressure of self-consolidating concrete exposed to fire. Constr Build Mater 2016;113:456–69. https://doi.org/10.1016/j.conbuildmat.2016.03.070.
[25] Liu J-C, Tan KH, Yao Y. A new perspective on nature of fire-induced spalling in concrete. Constr Build Mater 2018;184:581–90. https://doi.org/10.1016/j.conbuildmat.2018.06.204.
[26] Bažant ZP, Thonguthai W. Pore pressure in heated concrete walls: theoretical prediction. Mag Concr Res 1979;31:67–76. https://doi.org/10.1680/macr.1979.31.107.67.
[27] Bangi MR, Horiguchi T. Pore pressure development in hybrid fibre-reinforced high strength concrete at elevated temperatures. Cem Concr Res 2011;41:1150–6. https://doi.org/10.1016/j.cemconres.2011.07.001.
[28] Bangi MR, Horiguchi T. Effect of fibre type and geometry on maximum pore pressures in fibre-reinforced high strength concrete at elevated temperatures. Cem Concr Res 2012;42:459–66. https://doi.org/10.1016/j.cemconres.2011.11.014.
[29] Chen GM, Yang H, Lin CJ, Chen JF, He YH, Zhang HZ. Fracture behaviour of steel fibre reinforced recycled aggregate concrete after exposure to elevated temperatures. Constr Build Mater 2016;128:272–86. https://doi.org/10.1016/j.conbuildmat.2016.10.072.
[30] Li Y, Pimienta P, Pinoteau N, Tan KH. Effect of aggregate size and inclusion of polypropylene and steel fibers on explosive spalling and pore pressure in ultra-high-performance concrete (UHPC) at elevated temperature. Cem Concr Compos 2019;99:62–71. https://doi.org/10.1016/j.cemconcomp.2019.02.016.
[31] Ozawa M, Uchida S, Kamada T, Morimoto H. Study of mechanisms of explosive spalling in high-strength concrete at high temperatures using acoustic emission. Constr Build Mater 2012;37:621–8. https://doi.org/10.1016/j.conbuildmat.2012.06.070.

[32] Debicki G, Haniche R, Delhomme F. An experimental method for assessing the spalling sensitivity of concrete mixture submitted to high temperature. Cem Concr Compos 2012;34:958–63. https://doi.org/10.1016/j.cemconcomp.2012.04.002.
[33] Kalifa P, Menneteau F-D, Quenard D. Spalling and pore pressure in HPC at high temperatures. Cem Concr Res 2000;30:1915–27. https://doi.org/10.1016/S0008-8846(00)00384-7.
[34] Dong X, Ding Y, Wang T. Spalling and mechanical properties of fiber reinforced high-performance concrete subjected to fire. J Wuhan Univ Technol-Mater Sci Ed 2008;23:743–9.
[35] Peng G-F, Huang Z-S. Change in microstructure of hardened cement paste subjected to elevated temperatures. Constr Build Mater 2008;22:593–9. https://doi.org/10.1016/j.conbuildmat.2006.11.002.
[36] Kalifa P, Chéné G, Gallé C. High-temperature behaviour of HPC with polypropylene fibres: From spalling to microstructure. Cem Concr Res 2001;31:1487–99. https://doi.org/10.1016/S0008-8846(01)00596-8.
[37] Bilodeau A, Kodur VKR, Hoff GC. Optimization of the type and amount of polypropylene fibres for preventing the spalling of lightweight concrete subjected to hydrocarbon fire. Cem Concr Compos 2004;26:163–74. https://doi.org/10.1016/S0958-9465(03)00085-4.
[38] Han C-G, Hwang Y-S, Yang S-H, Gowripalan N. Performance of spalling resistance of high performance concrete with polypropylene fiber contents and lateral confinement. Cem Concr Res 2005;35:1747–53. https://doi.org/10.1016/j.cemconres.2004.11.013.
[39] Heo Y-S, Sanjayan JG, Han C-G, Han M-C. Relationship between inter-aggregate spacing and the optimum fiber length for spalling protection of concrete in fire. Cem Concr Res 2012;42:549–57. https://doi.org/10.1016/j.cemconres.2011.12.002.
[40] Chandra S, Berntsson L, Anderberg Y. Some effects of polymer addition on the fire resistance of concrete. Cem Concr Res 1980;10:367–75.
[41] Hertz KD, Sørensen LS. Test method for spalling of fire exposed concrete. Fire Saf J 2005;40:466–76.
[42] Khoury GA, Willoughby B. Polypropylene fibres in heated concrete. Part 1: Molecular structure and materials behaviour. Mag Concr Res 2008;60:125–36. https://doi.org/10.1680/macr.2008.60.2.125.
[43] Li Y, Tan KH, Yang E-H. Influence of aggregate size and inclusion of polypropylene and steel fibers on the hot permeability of ultra-high performance concrete (UHPC) at elevated temperature. Constr Build Mater 2018;169:629–37. https://doi.org/10.1016/j.conbuildmat.2018.01.105.
[44] Hager I, Mróz K. Role of Polypropylene Fibres in Concrete Spalling Risk Mitigation in Fire and Test Methods of Fibres Effectiveness Evaluation. Materials 2019;12:3869. https://doi.org/10.3390/ma12233869.
[45] Hager I, Mróz K, Tracz T. Contribution of polypropylene fibres melting to permeability change in heated concrete - the fibre amount and length effect. IOP Conf Ser Mater Sci Eng 2019;706:012009. https://doi.org/10.1088/1757-899X/706/1/012009.
[46] Shen L, Yao X, Di Luzio G, Jiang M, Han Y. Mix optimization of hybrid steel and polypropylene fiber-reinforced concrete for anti-thermal spalling. J Build Eng 2023;63:105409. https://doi.org/10.1016/j.jobe.2022.105409.

[47] Khoury GA. Polypropylene fibres in heated concrete. Part 2: Pressure relief mechanisms and modelling criteria. Mag Concr Res 2008;60:189–204. https://doi.org/10.1680/macr.2007.00042.
[48] Askarinejad Sina, Rahbar Nima. Effects of Cement–Polymer Interface Properties on Mechanical Response of Fiber-Reinforced Cement Composites. J Nanomechanics Micromechanics 2017;7:04017002. https://doi.org/10.1061/(ASCE)NM.2153-5477.0000119.
[49] European Committee for Standardization. Eurocode 2: Design of Concrete Structures - Part 1-2: General Rules - Structural Fire Design. 2004.
[50] Maluk C, Bisby L, Terrasi GP. Effects of polypropylene fibre type and dose on the propensity for heat-induced concrete spalling. Eng Struct 2017;141:584–95. https://doi.org/10.1016/j.engstruct.2017.03.058.
[51] Suhaendi SL, Horiguchi T. Effect of short fibers on residual permeability and mechanical properties of hybrid fibre reinforced high strength concrete after heat exposition. Cem Concr Res 2006;36:1672–8. https://doi.org/10.1016/j.cemconres.2006.05.006.
[52] Bei S, Zhixiang L. Investigation on spalling resistance of ultra-high-strength concrete under rapid heating and rapid cooling. Case Stud Constr Mater 2016;4:146–53. https://doi.org/10.1016/j.cscm.2016.04.001.
[53] Afroughsabet V, Ozbakkaloglu T. Mechanical and durability properties of high-strength concrete containing steel and polypropylene fibers. Constr Build Mater 2015;94:73–82. https://doi.org/10.1016/j.conbuildmat.2015.06.051.
[54] Widodo S. Fresh and hardened properties of Polypropylene fiber added Self-Consolidating Concrete. Int J Civ Struct Eng 2012;3:85.
[55] Lu F, Fontana M. Effects of Polypropylene Fibers on Preventing Concrete Spalling in Fire. Struct Fire 2016.
[56] Heo Y-S, Sanjayan JG, Han C-G, Han M-C. Limited effect of diameter of fibres on spalling protection of concrete in fire. Mater Struct 2012;45:325–35. https://doi.org/10.1617/s11527-011-9768-z.
[57] Maluk C, Bisby L, Krajcovic M, Torero JL. A Heat-Transfer Rate Inducing System (H-TRIS) Test Method. Fire Saf J 2016. https://doi.org/10.1016/j.firesaf.2016.05.001.
[58] Carlton A, Guo Q, Ma S, Quiel SE, Naito CJ. Experimental assessment of explosive spalling in normal weight concrete panels under high intensity thermal exposure. Fire Saf J 2022;134:103677. https://doi.org/10.1016/j.firesaf.2022.103677.
[59] EN T. 14889-1.(2006). Fibres for concrete-Part 1: Steel fibres-Definitions, specifications and conformity. 2006.
[60] A01 Committee. Specification for Steel Fibers for Fiber-Reinforced Concrete. ASTM International; n.d. https://doi.org/10.1520/A0820_A0820M-22.
[61] ASTM International. ASTM C39 Standard Test Method for Compressive Strength of Cylindrical Concrete Specimens. 2015. https://doi.org/10.1520/C0039.
[62] Ouyang Z, Zheng H, Patmanidis C, Naito C, Quiel S, Mooney M. Full-scale testing of precast tunnel lining segments under thrust jack loading: Design limits and ultimate response. Tunn Undergr Space Technol 2023;142:105446.
[63] ISO I. 22007-2 Plastics—Determination of Thermal Conductivity and Thermal Diffusivity—Part 2: Transient Plane Heat Source (Hot Disc) Method. ISO Geneva Switz 2015.
[64] Hot Disk Instruments. TPS 2500 S Hot Disk Thermal Constants Analyser 2020. https://www.hotdiskinstruments.com/products-services/instruments/tps-2500-s/.

[65] ASTM International. ASTM C642 Standard Test Method for Density, Absorption, and Voids in Hardened Concrete. 2013. https://doi.org/10.1520/C0642-13.
[66] Tramex. User Guide: Tramex CMEX II concrete moisture meter (digital) 2022. https://tramexmeters.com/perch/resources/downloads/user-guides/cmex2-rowus-online-user-guide.pdf.
[67] ASTM International. ASTM F2170 Standard Test Method for Determining Relative Humidity in Concrete Floor Slabs Using in situ Probes. 2019. https://doi.org/10.1520/F2170-19A.
[68] ASTM International. ASTM Standard E119-16 Standard Test Methods for Fire Tests of Building Construction and Materials. West Conshohocken, PA: 2016.
[69] Malz S, Sindersberger D, Monkman G, Steffens O, Kusterle W. Determination of the Water Content within Tunnel Linings to Assess Fire Safety 2023. https://doi.org/10.2139/ssrn.4390700.
[70] NFPA. NFPA 502: Standard for road tunnels, bridges, and other limited access highways. Quincy, MA: National Fire Protection Association; 2020.
[71] ASTM International. ASTM E1529 Standard Test Methods for Determining Effects of Large Hydrocarbon Pool Fires on Structural Members and Assemblies. West Conshohocken, PA: 2016.
[72] Guo Q, Root KJ, Carlton A, Quiel SE, Naito CJ. Framework for rapid prediction of fire-induced heat flux on concrete tunnel liners with curved ceilings. Fire Saf J 2019;109:102866. https://doi.org/10.1016/j.firesaf.2019.102866.
[73] Hukseflux. User Manual SBG01: Water cooled heat flux sensor Version 2023 2020. https://www.hukseflux.com/uploads/product-documents/SBG01_manual_v2023.pdf.
[74] FluxTeq. High Temperature Heat Flux Sensor (HTHFS-01) 2022. https://www.fluxteq.com/hthfs-high-temperature-heat-flux-sensor-1 (accessed July 15, 2022).
[75] Lo Monte F, Felicetti R, Rossino C. Fire spalling sensitivity of high-performanceconcrete in heated slabs under biaxial compressive loading. Mater Struct 2019;52:14. https://doi.org/10.1617/s11527-019-1318-0.

APPENDIX A – TECHNOLOGY TRANSFER ACTIVITIES

1 Accomplishments

- Concrete panels reinforced with steel fibers were subjected to spall experiments under fire condition.
- An evaluation was conducted on three types of concrete panels, each reinforced with varying amounts and lengths of polypropylene fibers, to assess their performance in representative hydrocarbon fuel fire scenarios.

1.1 What was done? What was learned?

- Eight concrete panel specimens were tested: 2 with a mix ratio identical to that currently used in concrete tunnel linings, 2 incorporated with 2 kg/m³ of 6 mm fibers sourced from Bekaert, 2 with 1 kg/m³ of 6 mm fibers also from Bekaert, and two with 1 kg/m³ of 19 mm fibers provided by Nycon.
- In the control group, the two panels exhibited intense spalling within the first 2 minutes of heating. Furthermore, spalling continued throughout the entire 2.5-minute duration of the heating period.
- The addition of polypropylene fibers significantly reduces the likelihood of spalling occurring in concrete. However, the effectiveness of these fibers is influenced by factors such as the amount and length of the fibers added. During a 1-hour exposure to an ASTM E1529 hydrocarbon fire, one of the panels with 1 kg/m³ of 6 mm long polypropylene fibers experienced very minor spalling, while the other panel with the same composition showed no spalling. The remaining four panels, all of which were also reinforced with polypropylene fibers, did not exhibit any spalling throughout the duration of the test.
- Due to the use of limestone as the coarse aggregate in the concrete, a phenomenon known as post-cooling spall was observed. This was characterized by the gradual peeling and flaking off of the concrete surface after cooling,

1.2 How have the results been disseminated?

A Journal paper is under development.

2 Participants and Collaborating Organizations

Name: Saidong Ma

Location: Lehigh University
Contribution: Primary experimental development and execution, manuscript lead, and corresponding author

Name: Spencer Quiel
Location: Lehigh University
Contribution: Research funding principle investigator, experimental and manuscript development

Name: Clay Naito
Location: Lehigh University
Contribution: Research funding principle investigator, experimental and manuscript development

3 Outputs

Journal publications (1 - under development)

Major reports (1 – UTC final report)

4 Outcomes/Impacts

This research involved experimental evaluations of concrete infused with both polypropylene and steel fibers, as well as concrete with only steel fibers. The results from these experiments provide crucial data for the future application of polypropylene fibers in tunnel linings. This data will be instrumental in subsequent comparative analyses with other fire protection strategies, such as sprayed fire-resistive materials (SFRM) and intumescent coatings, to determine the most effective methods for enhancing fire resistance in tunnel constructions.